Origin of Self-Assembled Helical Supramolecular Structures in Achiral C6 Biphenyl Carboxylic Acid Compounds

Kwang-Un Jeong,[†] Brian S. Knapp,[†] Jason J. Ge,[†] Shi Jin,[‡] Matthew J. Graham,[†] Frank W. Harris,[†] and Stephen Z. D. Cheng*,[†]

Maurice Morton Institute and Department of Polymer Science, The University of Akron, Akron, Ohio 44325-3909, and Department of Chemistry, College of Staten Island, The City University of New York, Staten Island, New York 10314

Received August 22, 2005. Revised Manuscript Received December 2, 2005

To understand the formation mechanism of helical supramolecular structures in the smectic C (SmC) liquid crystalline (LC) phase of BPCA-C*n*-P*m*OH (*n* is the number of methylene units, $n = 6-10$) (see: Jeong, K.-U.; Jin, S.; Ge, J. J.; Knapp, B. S.; Graham, M. J.; Ruan, J.; Guo, M.; Xiong, H.; Harris, F. W.; Cheng, S. Z. D. *Chem. Mater*. **2005**, *17*, 2852), a series of newly designed achiral C6 4-biphenyl carboxylic acid compounds was synthesized, of which all of them have six methylene units ($n = 6$). To recognize the importance of hydrogen (H)-bonding between hydroxyl groups and the small kink at the end of the phenyl groups, the hydroxyl group at the meta-position of phenyl groups in BPCA-C6-P*m*OH was first moved to the para-position to become BPCA-C6-P*p*OH, and then changed to a methoxy group to become BPCA-C6-P*m*OH_3. BPCA-C6-P, having no functional groups on the phenyl groups, was also synthesized. Finally, one more compound was synthesized to disrupt the formation of the H-bonded head-to-head dimers by replacing the H group on the carboxylic acid with an ethyl group to become BPCE-C6-P*m*OH. Phase structures of this series of compounds were characterized by wide-angle X-ray diffraction (WAXD), selected area electron diffraction, and differential scanning calorimetry. The phase identifications were also supported by the observation of morphological changes via polarized light microscopy. The formation of H-bonds between carboxylic acids as well as between hydroxyl groups was also studied using infrared spectroscopy (FT-IR). The two-dimensional WAXD along with the FT-IR experiments allowed us to understand the existence and stabilization of the synclinically tilted SmC (SmC_S) phase in the cases of BPCA-C6-P*m*OH and BPCA-C6-P*p*OH. In both cases, dimers can form H-bonds between the hydroxyl groups at the end of the dimers in the SmC_S phases. In the cases of BPCA-C6-P*m*OH_3 and BPCA-C6-P, they packed into an anticlinically tilted SmC (SmC_A) phase. Except for BPCE-C6-P*m*OH, this series of compounds formed helical supramolecular structures in the SmC phases similar to those of BPCA-C*n*-P*m*OH, regardless of whether their dimers were packed into synclinically or anticlinically tilted SmC phases. Therefore, the construction of the dimers was essential to form stable helical structures, but the −OH or $-OCH_3$ groups at the meta- or para-position of the phenyl groups were not critical. Computer simulation results indicated that the head-to-head dimers possessed a twist rather than a bent conformation. These could be the chemical origin of the helical supramolecular structures. Furthermore, the physical origin of the helical structure could be the dimer tilting toward the long axis of LC cylinders in the SmA networks during the transition from the SmA to SmC phases. This dimer tilting led to an elongation of the LC cylinders along their long axis and a decrease in the diameter of the cylinders. Since the cylinder lengths are fixed in the SmA networks, a mechanical compression was generated on the cylinders to force them to be twisted when the compounds entered the SmC phase.

Introduction

Liquid crystalline (LC) materials have been studied for several decades in electrical, optical, and life science fields not only for scientific interests but also for their practical applications. Formation of LC phases relies on mesogenic groups having either rodlike or disklike shapes.[2−5] These basic molecular structures can be further modified giving rise to controlled structural features of the mesophases.[6−8] In the past decade, one of the interesting new designs in the

* To whom correspondence should be addressed. E-mail: scheng@uakron.edu.
[†] The University of Akron.
[‡] The City University of New York, Staten Island.

(1) Jeong, K.-U.; Jin, S.; Ge, J. J.; Knapp, B. S.; Graham, M. J.; Ruan, J.; Guo, M.; Xiong, H.; Harris, F. W.; Cheng, S. Z. D. *Chem. Mater*. **2005**, *17*, 2852.
(2) Demus, D. *Handbook of Liquid Crystals*; Demus, D., Goodby, J., Gray, G. W., Spiess, H.-W., Vill, V., Eds.; Wiley-VCH: Weinheim, Germany, 1998; Vol. 1, pp 133−187.
(3) Goodby, J. W. *Handbook of Liquid Crystals*; Demus, D., Goodby, J., Gray, G. W., Spiess, H.-W., Vill, V., Eds.; Wiley-VCH: Weinheim, Germany, 1998; Vol. 2A, pp 3−21.
(4) Cammidge, A. N.; Bushby, R. J. *Handbook of Liquid Crystals*; Demus, D., Goodby, J., Gray, G. W., Spiess, H.-W., Vill, V., Eds.; Wiley-VCH: Weinheim, Germany, 1998; Vol. 2B, pp 693−748.
(5) Chandrasekhar, S. *Handbook of Liquid Crystals*; Demus, D., Goodby, J., Gray, G. W., Spiess, H.-W., Vill, V., Eds.; Wiley-VCH: Weinheim, Germany, 1998; Vol. 2B, pp 749−780.
(6) Kitzerow, H.-S.; Bahr, C. *Chriality in Liquid Crystals*; Kitzerow, H.-S., Bahr, C., Eds.; Springer: London, 2001; pp 1−27.
(7) Imrie, C. T.; Luckhurst, G. R. *Handbook of Liquid Crystals*; Demus, D., Goodby, J., Gray, G. W., Spiess, H.-W., Vill, V., Eds.; Wiley-VCH: Weinheim, Germany, 1998; Vol. 2B, pp 801−834.

10.1021/cm0518832 CCC: $33.50
Published on Web 01/05/2006

molecular architecture of LCs is the bent-core LC molecules (so-called "bow-shaped" or "banana-shaped" molecules) with a bent geometry at the center of the mesogenic unit.[9−27]

The most fascinating results observed in these bent-core achiral LC molecules are helical structures in the B7 phase[9−18] and the spontaneous macroscopic electric polarization in the B2 phase.[19−27] The helical structure of these LCs is generated when molecular interaction is weak and thermal fluctuation is extensive. The handedness is equally right- and left-handed due to the absence of molecular chirality. These chiral characteristics were previously thought to only originate from chiral molecules containing molecular chirality in the SmC* phase.[28−35] This unusual behavior of the achiral bent-core molecules was thought to be due to the geometric anisotropy ("banana"-like shape) of the LC molecule.[9−27] Later on, hockey stick-shaped molecules containing a bend at the end of mesogen,[36] twin molecules having a flexible link,[37] and amphiphilic block copolymers[38] were also found to show helical structures. Various origins of helical structures from achiral bent-core molecules were proposed including the tilting of molecules with respect to the layer normal which leads to an enantiomorphic structure,[20,21] twisting molecular directors that escape spontaneous polarization,[16] periodic polarization-modulated stripes together with layer undulation,[17] and/or the existence of axial conformers.[15,16,18]

One of the new ideas in the development of helical supramolecular structures is to self-assemble achiral molecules through noncovalent interactions.[39−49] Among noncovalent interactions, hydrogen (H)-bonding has become a major research topic due to its moderate bonding energy (10−50 kJ/mol), directionality, selectivity, and reversibility.[42−49] Up to now, not only rodlike and disklike LCs, but also polymeric LCs with side chain, main chain, network, and guest−host structures have been prepared by molecular self-assembly through the intra- or intermolecular H-bonding formations between H donors and H acceptors.[44,45]

We recently reported a three-dimensional (3D) helical supramolecular structure in the SmC phase of a series of 4-biphenyl carboxylic acid compounds (abbreviated as BPCA-C*n*-P*m*OH, here *n* is the number of methylene units; $n = 6-10$) having neither a molecular chirality nor a significant bent-core.[1] It was found that this series of compounds forms dimers via H-bonding between carboxylic acid groups. The question remains: what is the formation mechanism of the helical supramolecular structure in achiral BPCA-C*n*-P*m*OH?

The objective of this research is to identify the chemical and physical origins of the formation of the helical supramolecular structures. In particular, we speculated that the H-bonding between hydroxyl groups, the small kink at the end of the phenyl groups, and the H-bonding at carboxylic acids to form dimers are critical in forming these helical supramolecular structures.[1] To prove our speculations and understand the effect of each of these functional groups on the helical structures, a series of newly designed achiral C6 biphenyl carboxylic acid compounds was synthesized. All of these compounds possessed six methylene units ($n = 6$), yet the hydroxyl group at the meta-position of the phenyl ring in BPCA-C6-P*m*OH was first moved to the para-position to become BPCA-C6-P*p*OH, and then changed to a methoxy

(8) Nguyen, H.-T.; Destrade, C.; Malthête, J. *Handbook of Liquid Crystals*; Demus, D., Goodby, J., Gray, G. W., Spiess, H.-W., Vill, V., Eds.; Wiley-VCH: Weinheim, Germany, 1998; Vol. 2B, pp 865−886.
(9) Sekine, T.; Niori, T.; Watanabe, J.; Furukawa, T.; Choi, S. W.; Takezoe, H. *J. Mater. Chem.* **1997**, *7*, 1307.
(10) Pelzl, G.; Diele, S.; Jákli, A.; Lischka, C.; Wirth, I.; Weissflog, W. *Liq. Cryst.* **1999**, *26*, 135.
(11) Lee, C. K.; Chien, L. C. *Liq. Cryst.* **1999**, *26*, 609.
(12) Pelzl, G.; Diele, S.; Weissflog, W. *Adv. Mater.* **1999**, *11*, 707.
(13) Jákli, A.; Lischka, C. H.; Weissflog, W.; Pelzl, G.; Saupe, A. *Liq. Cryst.* **2000**, *27*, 1405.
(14) Weissflog, W.; Nádasi, H.; Dunemann, U.; Pelzl, G.; Diele, S.; Eremin, A.; Kresse, H. *J. Mater. Chem.* **2001**, *11*, 2748.
(15) Thisayukta, J.; Nakayama, Y.; Kawauchi, S.; Takezoe, H.; Watanabe, J. *J. Am. Chem. Soc.* **2000**, *122*, 7441.
(16) Thisayukta, J.; Niwano, H.; Takezoe, H.; Watanabe, J. *J. Am. Chem. Soc.* **2002**, *124*, 3354.
(17) Coleman, D. A.; Fernsler, J.; Chattham, N.; Nakata, M.; Takanishi, Y.; Körblova, E.; Link, D. R.; Shao, R.-F.; Jang, W. G.; Maclennan, J. E.; Mondainn-Monval, O.; Boyer, C.; Weissflog, W.; Pelzl, G.; Chien, L.-C.; Zasadzinski, J.; Watanabe, J.; Walba, D. M.; Takezoe, H.; Clark, N. A. *Science* **2003**, *301*, 1204.
(18) Kajitani, T.; Masu, H.; Kohmoto, S.; Yamanoto, M.; Yamaguchi, K.; Kishikawa, K. *J. Am. Chem. Soc.* **2005**, *127*, 1124.
(19) Niori, T.; Sekine, T.; Watanabe, J.; Furukawa, T.; Takezoe, H. *J. Mater. Chem.* **1996**, *6*, 1231.
(20) Link, D. R.; Natale, G.; Shao, R.; Mclennan, J. E.; Clark, N. A.; Korblova, E.; Walba, D. M. *Science* **1997**, *278*, 1924.
(21) Heppke, G.; Moro, D. *Science* **1998**, *279*, 1872.
(22) Zennyoji, M.; Takanishi, Y.; Ishikawa, K.; Thisayukta, J.; Watanabe, J.; Takezoe, H. *J. Mater. Chem.* **1999**, *9*, 2775.
(23) Walba, D. M.; Körblova, E.; Shao, R.; Maclennam, J. E.; Link, D. R.; Glaser, M. A.; Clark, N. A. *Science* **2000**, *288*, 2181.
(24) Shen, D.; Pegenau, A.; Diele, S.; Wirth, I.; Tschierske, C. *J. Am. Chem. Soc.* **2000**, *122*, 1593.
(25) Goodby, J. W.; Bruce, D. W.; Hird, M.; Imrie, C.; Neal, M. *J. Mater. Chem.* **2001**, *11*, 2631.
(26) Nakata, M.; Link, D. R.; Thisayukta, J.; Takanishi, Y.; Ishikawa, K.; Watanabe, J.; Takezoe, H. *J. Mater.* Chem. **2001**, *11*, 2694.
(27) Kobayashi, S.; Hamasaki, N.; Suzuki, M.; Kimura, M.; Shirai, H.; Hanabusa, K. *J. Am. Chem. Soc.* **2002**, *124*, 6550.
(28) Mason, S. F. *Nature* **1984**, *311*, 19.
(29) Goodby, J. W. *Science* **1986**, *231*, 350.
(30) Barton, J. K. *Science* **1986**, *233*, 727.
(31) Katsaras, J.; Raghunathan, V. A. *Phys. Rev. Lett.* **1995**, *74*, 2022.
(32) Selinger, J. V.; MacKintosh, F. C.; Schnur, J. M. *Phys. Rev. E* **1996**, *53*, 3804.
(33) Li, C. Y.; Cheng, S. Z. D.; Weng, X.; Ge, J. J.; Bai, F.; Zhang, J. Z.; Calhoun, B. H.; Harris, F. W.; Chien, L. C.; Lotz, B. *J. Am. Chem. Soc.* **2001**, *123*, 2462.
(34) Li, C. Y.; Ge, J. J.; Bai, F.; Calhoun, B. H.; Harris, F. W.; Cheng, S. Z. D.; Chien, L. C.; Lotz, B.; Keith, H. D. *Macromolecules* **2001**, *34*, 3634.
(35) Lotz, B.; Cheng, S. Z. D. *Polymer* **2005**, *46*, 577 and references therein.
(36) Hird, M.; Goodby, J. W.; Gough, N.; Toyne, K. J. *J. Mater. Chem.* **2001**, *11*, 2732.
(37) Takanishi, Y.; Izumi, T.; Watanabe, J.; Ishikawa, K.; Takezoe, H.; Iida, A. *J. Mater. Chem.* **1999**, *9*, 2771.
(38) Cornelissen, J. J. L. M.; Rowan, A. E.; Nolte, R. J. M.; Sommerdijk, N. A. J. M. *Chem. Rev.* **2001**, *101*, 4039.
(39) Hunter, C. A.; Sanders, J. K. M. *J. Am. Chem. Soc.* **1990**, *112*, 5525.
(40) Lehn, J. M. *Science* **2002**, *295*, 2400.
(41) Messmore, B. W.; Sukerkar, P. A.; Stupp, S. I. *J. Am. Chem. Soc.* **2005**, *127*, 7992.
(42) Yang, W.; Chai, X.; Chi, L.; Liu, X.; Cao, Y.; Lu, R.; Jiang, Y.; Tang, X.; Fuchs, H.; Li, T. *Chem. Eur. J.* **1999**, *5*, 1144.
(43) Hirschberg, J. H.; Brunsveld, L.; Ramzi, A.; Vekemans, J. A.; Sijbesma, R. P.; Meijer, E. W. *Nature* **2000**, *407*, 167.
(44) Kato, T.; Mizoshita, N.; Kanie, K. *Macromol. Rapid Commun.* **2001**, *22*, 797.
(45) Kato, T. *Science* **2002**, *295*, 2414.
(46) Reinhoudt, D. N.; Drego-Calama, M. *Science* **2002**, *295*, 2403.
(47) Keinan, S.; Ratner, M. A.; Marks, T. J. *Chem. Mater.* **2004**, *16*, 1848.
(48) Xue, C.; Jin, S.; Weng, X.; Ge, J. J.; Shen, Z.; Shen, H.; Graham, M. J.; Jeong, K.-U.; Wang, H.; Zhang, D.; Guo, M.; Harris, F. W.; Cheng, S. Z. D.; Li, C. Y.; Zhu, L. *Chem. Mater.* **2004**, *16*, 1014.
(49) Jin, S.; Ma, Y.; Zimmerman, S. C.; Cheng, S. Z. D. *Chem. Mater.* **2004**, *16*, 2975.

group to become BPCA-C6-P*m*OCH$_3$, and finally to no substitution on the phenyl group (BPCA-C6-P). As a reference, one compound was also synthesized to disrupt the formation of the H-bonded dimer by replacing the H on carboxylic acid with an ethyl group (BPCE-C6-P*m*OH).

Phase structures and transition behaviors of this series of compounds were characterized with the combined techniques of differential scanning calorimetry (DSC), polarized light microscopy (PLM), wide-angle X-ray diffraction (WAXD), and selected area electron diffraction (SAED). The H-bonding formations between carboxylic acids as well as between hydroxyl groups were also studied using infrared spectroscopy (FT-IR). All the compounds which can construct head-to-head dimers via H-bonding between carboxylic acids formed helical supramolecular structures similar to those of BPCA-C*n*-P*m*OHs. Based on our experimental observations and the computer-calculated minimal free energy geometry of the dimer, we can conclude that the helical supramolecular structures in this series of compounds are resulted from the axial chiral conformers of individual head-to-head dimers (chemical origin) under a mechanical compression caused by dimer tilting with respect to the layer normal along the long axis of the SmA LC cylinders during the transition from the SmA to the SmC phases (physical origin).

Experimental Section

Materials and Sample Preparation. Achiral 4′-[6-(3′-hydroxyl-phenoxy)-hexyloxy]-4-biphenylcarboxylic acid (BPCA-C6-P*m*OH) connected with alkoxyl chains having six carbon numbers ($n = 6$) and terminated by phenyl groups with meta-positioned hydroxyl groups was synthesized using four step substitution reactions.[1] To understand the formation mechanism of the helical supramolecular structures from the BPCA-C*n*-P*m*OH compounds, a series of new compounds was designed and synthesized using similar procedures. All of these compounds had six methylene units ($n = 6$), yet the hydroxyl group at the meta-position of the phenyl ring was first changed to a methoxy function to become BPCA-C6-P*m*OCH$_3$ and moved to the para-position to become BPCA-C6-P*p*OH. The importance of H-bonding between hydroxyl groups and the small "kink" at the phenyl end group was studied with BPCA-C6-P containing no functions at the phenyl end group. Finally, one compound was also synthesized in order to disrupt the formation of dimers via H-bonding to change the H at the carboxylic acid with an ethyl group (BPCE-C6-P*m*OH). All the compounds were purified using column chromatography, followed by repeated crystallization, and their purity was confirmed using ^{1}H NMR along with thin-layer chromatography. The detailed synthetic procedures and purification methods can be found in the ref 50. The general chemical structures of the achiral C6 biphenyl carboxylic acid compounds are shown in Scheme 1.

For 1D WAXD measurements, structurally isotropic films with a thickness of about 0.5 mm were prepared by melting the compounds in an aluminum cell. Oriented samples obtained by mechanical shearing in the low-ordered SmC phase were used in 2D WAXD experiments for determining various phase structures after the samples were thermally treated at different temperatures. Thin film samples were prepared for transmission electron microscopy (TEM) experiments (used in the Supporting Information) by

Scheme 1

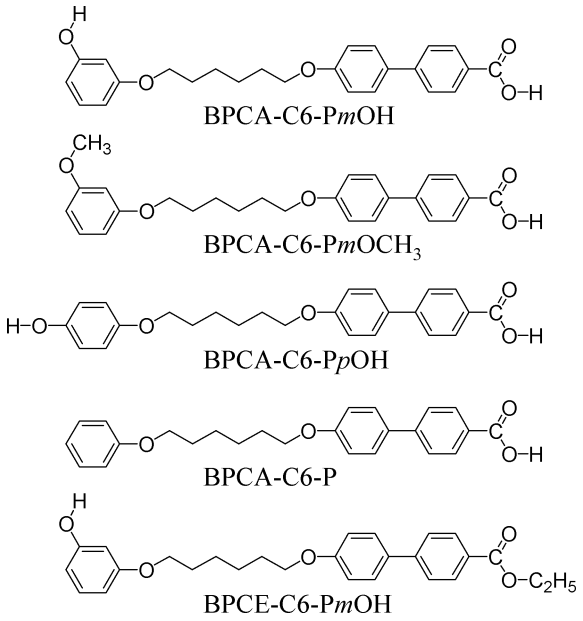

casting C6 compound/tetrahydrofuran solution (0.1 w/v %) on carbon-coated glass slides. After crystallization, the films were removed from the glass slide, floated on a water surface, and recovered using copper grids. The samples prepared for PLM had a thickness ranging from 1 to 5 μm, and they were melt-processed between two polyimide-coated/rubbed glass sides. The film samples for FT-IR measurements were the same as those used in PLM experiments, but the substrates were KBr plates.

Equipment and Experiments. The thermal behaviors of the phase transitions were studied using a Perkin-Elmer PYRIS Diamond DSC with an Intracooler 2P apparatus. The temperatures and heat flows were calibrated using material standards at cooling and heating rates ranging from 2.5 to 40 °C/min. The heating experiments always preceded the cooling experiments in order to eliminate previous thermal histories, and the cooling and heating rates were always kept identical. The transition temperatures were determined by measuring the onset and peak temperatures from both the cooling and heating scans at different rates.

1D WAXD experiments were conducted in the transmission mode of a Rigaku 12 kW rotating-anode X-ray (Cu Kα radiation) generator coupled to a diffractometer. The diffraction peak positions and widths were calibrated with silicon crystals of known crystal size in the high-2θ-angle region (>15°) and silver behenate in the low-2θ-angle region. A hot stage was coupled to the diffractometer in order to study the LC structural evolutions with temperature changes during heating and cooling. The temperature of this hot stage was calibrated to be within ±1 °C. Samples were scanned across a 2θ-angle range from 1.5° to 35° at a scanning rate of 4°/min. 2D WAXD patterns for the oriented samples were obtained using an imaging system (Rigaku, R-AXIS-IV) with an 18 kW rotating-anode X-ray generator. A hot stage was also used to obtain diffraction peaks from the LC structures at elevated temperatures. A 30 min exposure time was required for a high-quality pattern. In both 1D and 2D WAXD experiments, background scattering was subtracted from the sample scans.

TEM (FEI Tacnai 12) experiments (used in the Supporting Information) were carried out to examine crystal morphology using an accelerating voltage of 120 kV. Selected area electron diffraction (SAED) patterns of different zones within the samples were also obtained. Calibration of the SAED spacing smaller than 0.384 nm was carried out using evaporated thallous chloride, which has a

(50) Knapp, B. S. Ph.D. Dissertation, University of Akron, 2003.

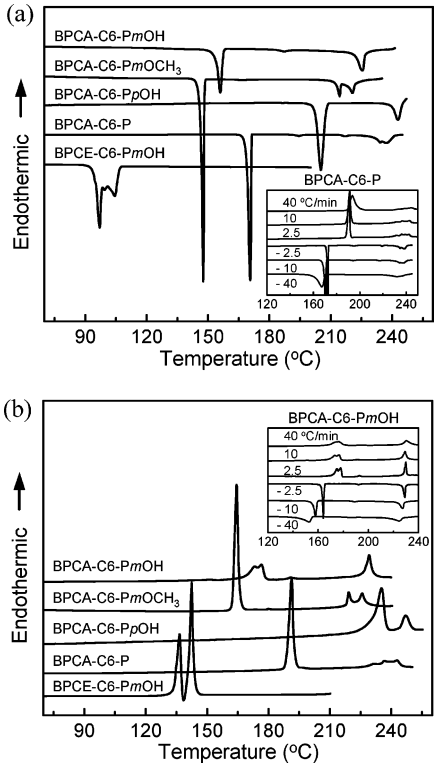

Figure 1. Set of DSC (a) cooling and (b) subsequent heating thermal diagrams for achiral C6 biphenyl model compounds at a rate of 2.5 °C/min. The two insets are DSC cooling and subsequent heating thermal diagrams for BPCA-C6-P (in part a) and BPCA-C6-P*m*OH (in part b) samples at different rates between 2.5 and 40 °C/min.

largest first-order spacing diffraction of 0.384 nm. Spacing values larger than 0.384 nm were calibrated by doubling the *d*-spacing values of the first-order diffractions.

Optical LC textures of the LC phases at different temperatures were observed with a PLM (Olympus BH-2) coupled with a calibrated Mettler heating stage (FP-90). The H-bond formations between carboxylic acids and between hydroxyl groups were studied using an FT-IR (Digilab Win-IR Pro FTS 3000) equipped with a Bruker heating stage. The temperatures of this hot stage were calibrated to be within ±0.5 °C. Overlapped C═O absorption peaks in FT-IR were resolved using the PeakFit peak separation program (Jandel Scientific). The Cerius^2 (version 4.6) simulation software from Accelrys was used to calculate the head-to-head dimer minimal energy geometry of the achiral C6 biphenyl carboxylic acid model compounds in the isolated gas phase utilizing the COMPASS force field.

Results and Discussion

Thermal Transitions and Their Corresponding Structural Changes. Multiple transition temperatures and the enthalpy changes at the transitions of the C6 biphenyl carboxylic acid compounds are observed as shown in Figure 1, parts a and b. It is evident that the compounds with a linear shape (BPCA-C6-P*p*OH and BPCA-C6-P) without a small "kink" at the phenyl groups show higher transition temperatures than those compounds having meta-positioned groups (BPCA-C6-P*m*OH and BPCA-C6-P*m*OCH_3) at the phenyl groups during cooling and subsequent heating (see Figure 1, parts a and b). Moreover, the compounds containing hydroxyl groups at the meta- or para-position of the phenyl rings (BPCA-C6-P*p*OH and BPCA-C6-P*m*OH) exhibit higher transition temperatures than those of compounds without hydroxyl groups at the phenyl rings (BPCA-C6-P and BPCA-C6-P*m*OCH_3), respectively. This could be due to the intermolecular H-bonding between hydroxyl groups at the ends of the phenyl rings. On the other hand, the BPCE-C6-P*m*OH compound, which cannot construct dimers via the intermolecular H-bonding between carboxylic acids (see below for the FT-IR results), does not show LC phases as confirmed by WAXD experiments.

Different cooling and subsequent heating rates were also used and are shown in the insets of Figure 1, parts a and b, for BPCA-C6-P and BPCA-C6-P*m*OH as two examples, respectively. The high-temperature transitions for both compounds do not exhibit cooling-rate dependence, and they are associated with the low-ordered LC phase transitions. The low-temperature transitions show small cooling-rate dependences, and they are representatives of highly ordered LC or crystalline phase transitions. These transition temperatures and enthalpy changes at the transitions during cooling at 2.5 °C/min are listed in Table 1.

Paralleling the DSC experiments, 1D WAXD cooling experiments at 2.5 °C/min for these compounds were carried out in order to obtain structural evolutions at different temperatures as shown in Figure 2, parts a and b, for BPCA-C6-P and BPCA-C6-P*m*OH as two examples, respectively. In both figures, structures with two different length scales can be identified. One structure is on the nanometer scale between $2\theta = 1.5°$ and 8°, and the other is on the subnanometer scale between 9° and 35°. For BPCA-C6-P, Figure 2a shows the structural changes which correspond to the five exothermic processes observed in the DSC cooling diagram (Figure 1a). At the isotropization temperature (T_i) of 241 °C, there is a sudden shift of the scattering halo in the WAXD patterns toward a higher 2θ angle from 18.8° to 19.0° (*d*-spacing from 0.472 to 0.467 nm) in Figure 2a, indicating a transition from the I phase to a low-ordered nematic (N) LC phase.[51−57] Slightly lower than 237 °C, the low-2θ-angle reflection appears at 1.95° ($d = 4.53$ nm), while the scattering halo at $2\theta = 19.0°$ shifts toward a 2θ angle of 19.4° ($d = 0.456$ nm). At 221 °C, a shift of the low-2θ-angle reflection to 2.59° ($d = 3.41$ nm) take place, coupled with a change of the amorphous halo from $2\theta = 19.4°$ to 19.7° ($d = 0.451$ nm) in the high-2θ-angle region. A sharpening of the halo in the high-2θ-angle region at 197 °C can also be observed. Finally, sharp reflections develop in the high-2θ-angle region, and reflection peaks in the low-2θ-angle region also change at 172 °C to form a crystalline

(51) Unger, G.; Feijoo, J. L.; Percec, V.; Yourd, R. *Macromolecules* **1991**, *24*, 953.
(52) Yandrasits, A.; Cheng, S. Z. D.; Zhang, A.; Cheng, J.; Wunderlich, B.; Percec, V. *Macromolecules* **1992**, *25*, 2112.
(53) Pardey, R.; Harris, F. W.; Cheng, S. Z. D.; Adduci, J.; Facinelli, J. V.; Lenz, R. W. *Macromolecules* **1992**, *25*, 5060.
(54) Pardey, R.; Shen, D.; Gabori, P. A.; Harris, F. W.; Cheng, S. Z. D.; Adduci, J.; Facinelli, J. V.; Lenz, R. W. *Macromolecules* **1993**, *26*, 3687.
(55) Yoon, Y.; Ho, R.-M.; Moon, B.; Kim, D.; McCreight, K. W.; Li, F.; Harris, F. W.; Cheng, S. Z. D.; Percec, V.; Chu, P. *Macromolecules* **1996**, *29*, 3421.
(56) Ge, J. J.; Zhang, A.; McCreight, K. W.; Ho, R.-M.; Wang, S.-Y.; Jin, X.; Harris, F. W.; Cheng, S. Z. D. *Macromolecules* **1997**, *30*, 6498.
(57) Zheng, R.-Q.; Chen, E.-Q.; Cheng, S. Z. D.; Xie, F.; Yan, D.; He, T.; Percec, V.; Chu, P.; Ungar, G. *Macromolecules* **1999**, *32*, 3574.

Table 1. Transition Temperatures and Enthalpies for the C6 Biphenyl Model Compounds[a]

compounds	transition temperature °C (enthalpy, kJ/mol) at 2.5 °C/min cooling
BPCA-C6-P*m*OH	K_M 162 (17.1) SmI_S 192 (0.8) SmC_S 224 (0.7) SmA 227 (1.5) N 229 (11.2) I
BPCA-C6-P*m*OCH_3	K_T 151 (34.1) SmI_A 174 (0.2) SmC_A 217 (0.7) SmA 222 (1.0) N 223 (10.2) I
BPCA-C6-P*p*OH	K_M 212 (27.8) SmI_S 229 (0.2) SmC_S 244 (0.6) SmA 246 (1.6) N 247 (9.0) I
BPCA-C6-P	K_O 172 (41.5) SmI_A 197 (1.0) SmC_A 221 (0.7) SmA 237 (5.9) N 241 (7.2) I
BPCE-C6-P*m*OH	K 105 (44.9) I

[a] Here, subscripts M, T, O, S, and A mean monoclinic, triclinic, orthorhombic, synclinic, and anticlinic, respectively. Merged peaks at the higher temperatures for BPCA-C6-P*m*OCH_3 and BPCA-C6-P*p*OH are resolved using the PeakFit peak separation program.

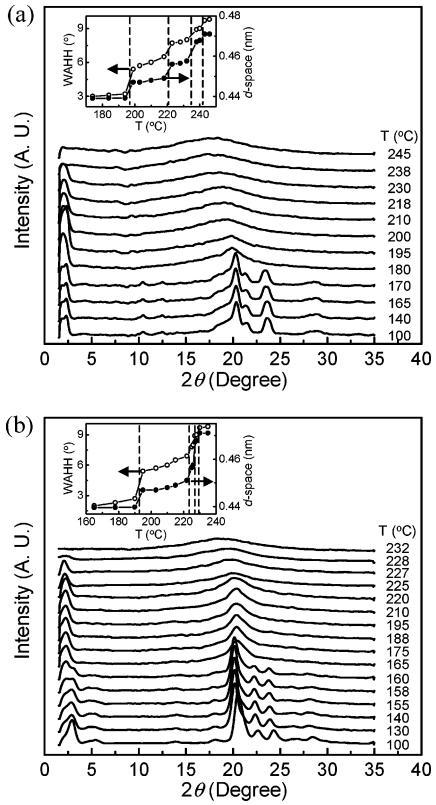

Figure 2. Two sets of 1D WAXD patterns of (a) BPCA-C6-P and (b) BPCA-C6-P*m*OH at a cooling rate of 2.5 °C/min at different temperatures. The two insets are the relationship between the *d*-spacings of the center scattering halos and the width at half-height of the scattering halos of BPCA-C6-P (in part a) and BPCA-C6-P*m*OH (in part b) samples with temperatures above the crystallization temperature. The vertical dash-lines are indications of the thermal transitions based on the DSC cooling results.

(K) phase, as shown in Figure 2a. In the case of BPCA-C6-P*m*OH, the I phase can be found above 229 °C. When passing through this T_i during cooling, the trend of phase transformations of BPCA-C6-P*m*OH is almost identical with those of BPCA-C6-P as shown in Figure 2b. First, three low-ordered LC phases evolve before one highly ordered LC phase, and finally the system enters a K phase at a lower temperature.

These structural changes in Figure 2, parts a and b, can be characterized by the *d*-spacings and the changes in the width at half-height (WAHH) of the scattering halos with respect to temperature before the reflection peaks appeared in the high-2θ-angle region.[55,56,58] The results are shown in the insets of Figure 2, parts a and b, for BPCA-C6-P and BPCA-C6-P*m*OH, respectively. The vertical dash-lines are indications of the thermal transitions based on the DSC cooling results. The changes of these structural parameters correspond well to those thermal transitions. Moreover, the WAXD patterns during heating are similar to those during cooling.

Phase transitions of other compounds (BPCA-C6-P*m*OCH_3 and BPCA-C6-P*p*OH) possess certain similarities with those of BPCA-C6-P and BPCA-C6-P*m*OH. On the other hand, the BPCE-C6-P*m*OH compound, which cannot construct a mesogen via the intermolecular H-bonding between carboxylic acids, only shows an I ↔ K phase transition at 105 °C. To identify the phase structure and know the detailed molecular packing in the ordered LC and crystalline phases, 2D WAXD from aligned samples and SAED obtained from single crystals are needed.

Since the major topic in this publication is the search for the origin of helical supramolecular structure formation in the SmC phases, the crystal and highly ordered LC structural determinations are not presented here but attached as Supporting Information for this publication (see the Supporting Information). The detailed crystal structure information is listed in Table 2.

Identifications of the Low-Ordered Liquid Crystal Phases and Dimer Tilting Arrangements. We are now focusing on two low-ordered LC phase identifications of this series of compounds which are associated with the helical supramolecular structure. Figure 3a shows the geometry of the mechanically sheared film sample and definitions of three directions along which the X-ray beam was aligned. Figure 3b is a 2D WAXD pattern of BPCA-C6-P*m*OH at 200 °C when the incident X-ray beam is along the edge direction. In this figure, a pair of scattering halos at $2\theta = 19.7°$ ($d = 0.451$ nm) is located in the second and fourth quadrants ($\theta = 50°$ counterclockwise out of the meridian). This illustrates the 40° clockwise synclinic dimer tilting layer-by-layer with respect to the layer normal toward the shear direction (*y*, S.D.), as shown in Figure 3d. Its correlation length is about 1.3 nm, estimated by the Scherrer equation,[55,56,58] representing liquidlike ordering within the layer. In addition, a pair of low-2θ-angle diffractions at $2\theta = 2.45°$ ($d = 3.60$ nm) can be clearly identified with a second-order diffraction at $2\theta = 4.91°$ in the inset of Figure 3b. This structure can thus be identified as a synclinically tilted SmC (SmC_S) phase as illustrated in Figure 3d. On the basis of the tilting angle (40°) and the measured layer thickness (3.60 nm), the length of dimer in the layer of this SmC_S phase is calculated to be 4.70 nm, which agrees well with the calculated length of the head-to-head dimer (4.73 nm). For BPCA-C6-P*p*OH in the low-ordered SmC phase, the dimers are also synclinically tilted layer-by-layer (Figure 3c). The structure of BPCA-C6-P*p*OH is thus also identified as a SmC_S phase. In both

(58) Seddon, J. M. *Handbook of Liquid Crystals*; Demus, D., Goodby, J., Gray, G. W., Spiess, H.-W., Vill, V., Eds.; Wiley-VCH: Weinheim, Germany, 1998; Vol. 1, pp 635−679.

Table 2. Crystal System, Axial System, and Density of C6 Biphenyl Carboxylic Acid Model Compounds at the Room Temperature

			axial system						density	
compound	dimer	crystal system	*a* (nm)	*b* (nm)	*c* (nm)	α (deg)	*β* (deg)	*γ* (deg)	exptl	calcd
BPCA-C6-P*m*OH	2	monoclinic	0.79	0.75	4.93	90.0	44.5	90.0	1.27	1.30
BPCA-C6-P*m*OCH$_3$	8	triclinic	0.53	3.12	5.83	83.5	90.0	88.0	1.17	1.20
BPCA-C6-P*p*OH	2	monoclinic	0.71	0.87	4.84	90.0	47.0	90.0	1.22	1.24
BPCA-C6-P	4	orthorhombic	0.64	0.74	8.71	90.0	90.0	90.0	1.26	1.27

cases, the H-bonding can be formed between hydroxyl groups at the ends of dimers.

On the other hand, BPCA-C6-P*m*OCH$_3$ (Figure 3e) and BPCA-C6-P (Figure 3f), which cannot form H-bonds between the layers, exhibit 2D WAXD patterns with two pairs of symmetric scattering halos with identical *d*-spacing (0.451 nm) and intensity in the four quadrants. The tilting angles for both compounds are ±44° and ±42°, respectively. Therefore, they may possess an anticlinic dimer tilting layer-by-layer as illustrated in Figure 3g, and they should be identified as a anticlinically tilted SmC (SmC$_A$) phases. However, parts e and f of Figure 3 do not warrant the SmC$_A$ chain packing, since this 2D WAXD pattern can also be constructed by a mixture of two SmC$_S$ domains with opposite chain tilting directions. This argument can be solved by the number of brushes in the schlieren textures of the SmC phases as previously reported.[59−61] The schlieren textures in SmC phases from C6 biphenyl carboxylic acid compounds are obtained between two glass slides with a thickness of less than 2 μm, as shown in Figure 4a−d. The schlieren textures of SmC$_S$ phases exhibit only four-brush defects (Figure 4, parts a and b, for BPCA-C6-P*m*OH and BPCA-C6-P*p*OH) because they cannot generate discontinuous defects planes which create two-brush defects. On the other hand, the schlieren textures of SmC$_A$ phases have two-brush and four-brush defects (Figure 4, parts c and d, for BPCA-

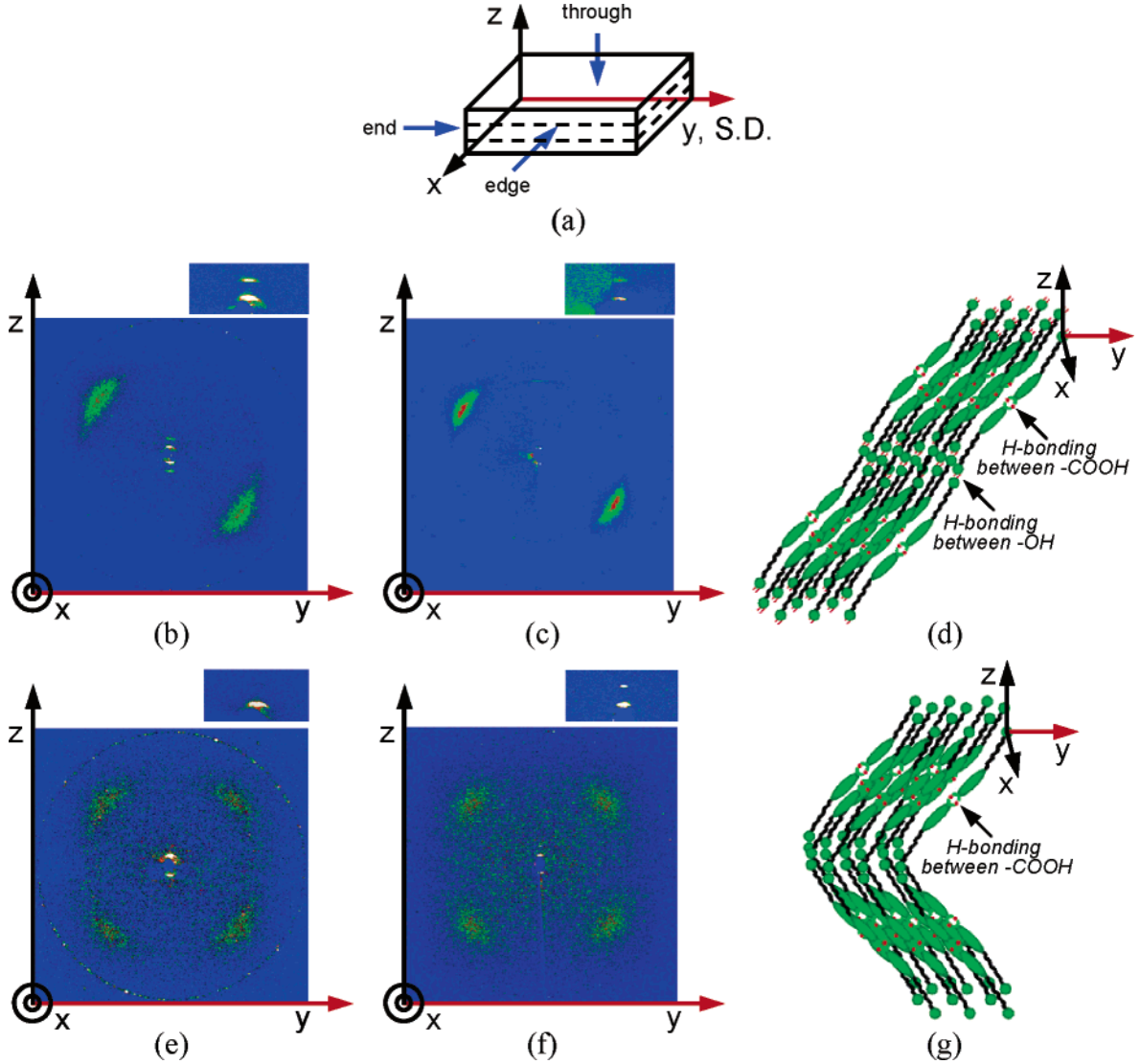

Figure 3. 2D WAXD patterns of the SmC phases when the X-ray beam is along the edge direction of mechanically sheared (b) BPCA-C6-P*m*OH, (c) BPCA-C6-P*p*OH, (e) BPCA-C6-P*m*OCH$_3$, and (f) BPCA-C6-P samples, and schematic illustrations of the molecular arrangement in the SmC layers for (d) BPCA-C6-P*m*OH and BPCA-C6-P*p*OH and (g) BPCA-C6-P*m*OCH$_3$ and BPCA-C6-P. The sheared sample geometry for the 2D WAXD is illustrated in (a).

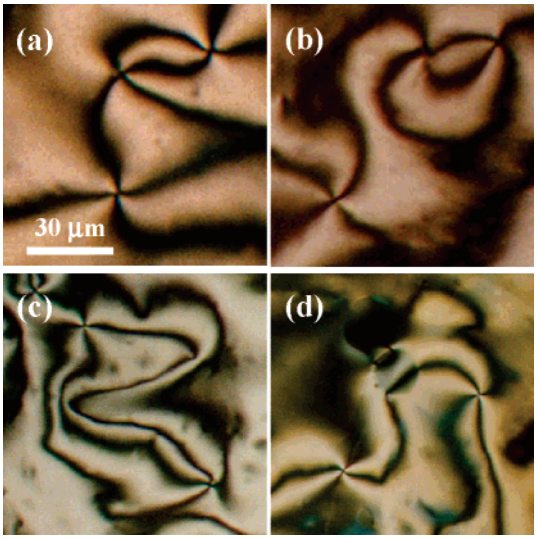

Figure 4. PLM schlieren textures in the SmC_S phases of (a) BPCA-C6-P*m*OH and (b) BPCA-C6-P*p*OH and in the SmC_A phases of (c) BPCA-C6-P*m*OCH_3 and (d) BPCA-C6-P.

C6-P*m*OCH_3 and BPCA-C6-P). The tilting types of dimers in the crystalline phase and highly ordered LC phase (see the Supporting Information) are also retained in their low-ordered SmC_S and SmC_A phase in these C6 biphenyl carboxylic acid compounds. It can be concluded that the H-bonding between hydroxyl groups at the ends of the dimers plays an important role to form the SmC_S phase (BPCA-C6-P*m*OH and BPCA-C6-P*p*OH). Without the H-bonding, only the SmC_A phase in BPCA-C6-P*m*OCH_3 and BPCA-C6-P can be found.

With increasing temperature, these compounds enter the SmA phase. For example, Figure 5a is a 2D WAXD pattern of BPCA-C6-P*m*OH at 226 °C when the incident X-ray beam is along the edge direction. In the high-2θ-angle region, a pair of scattering halos at $2\theta = 19.4°$ ($d = 0.456$ nm) is located on the equator with a correlation length of 1.2 nm. In addition, a pair of low-2θ-angle diffractions at $2\theta = 1.93°$ ($d = 4.58$ nm) can be clearly identified on the meridian with weak second-order diffraction at $2\theta = 3.86°$ in the inset of Figure 5a. This means that the average long axis of the dimers is parallel to the layer normal (z). Figure 5b shows a 2D WAXD pattern of BPCA-C6-P in the SmA phase. A very similar observation can be found as in Figure 5a. Therefore, this structure can be identified as a SmA phase as illustrated in Figure 5c. The length of the dimer in the layer of this SmA phase is 4.58 nm, which is shorter than the calculated length of the chain (4.73 nm). This difference may be due to the fact that the alkoxyl chains of BPCA-C6-P*m*OH in this SmA phase contain gauche and trans conformations instead of the assumed all-trans conformation in the calculation, which was confirmed by solid-state carbon-13 (^{13}C) nuclear magnetic resonance spectroscopy in a previous report.[1] The 2D WAXD fiber patterns of the other C6 biphenyl carboxylic acids are identical with that of BPCA-

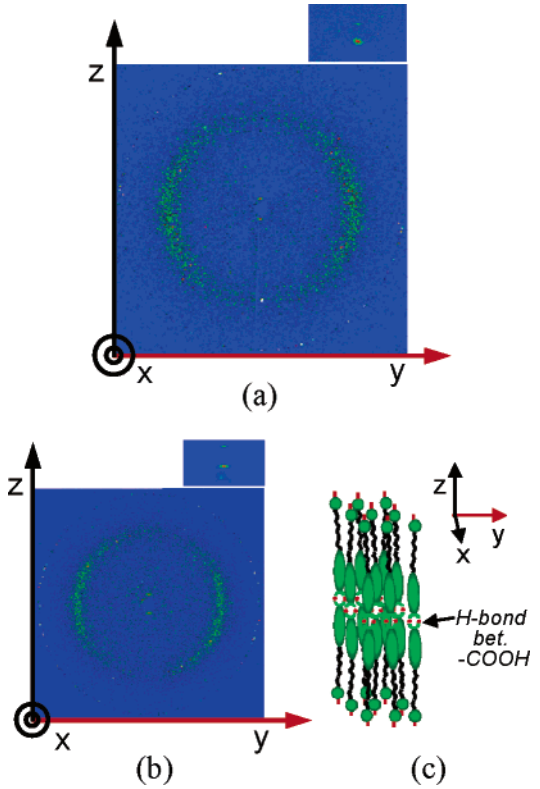

Figure 5. 2D WAXD patterns of the SmA phase when the X-ray beam is along the edge direction of mechanically sheared (a) BPCA-C6-P*m*OH and (b) BPCA-C6-P. The sheared sample geometry for the 2D WAXD is identical with that in Figure 3a. (c) Schematic illustration of molecular arrangement in the SmA layers.

C6-P*m*OH. The layer diffractions of the SmA phase for BPCA-C6-P and BPCA-C6-P*m*OCH_3 are at $2\theta = 1.95°$ ($d = 4.53$ nm), and the layer diffraction of BPCA-C6-P*p*OH is at $2\theta = 1.93°$ ($d = 4.58$ nm).

Hydrogen-Bonding Associations in the Phases. To understand the formation of head-to-head dimers assembled by intermolecular H-bonding between carboxylic acids and to find a driving force to form the synclinic or anticlinic dimer tilting between the neighboring layers in this series of compounds, FT-IR measurements were carried out in different phases, and the results are shown in Figure 6.

On the basis of the FT-IR results, the absorption band at 3560 cm^{-1} can be assigned to the stretching vibration of free O−H groups, while H-bonded O−H stretching bands appear between 3500 and 3200 cm^{-1}.[62] Both BPCA-C6-P*m*OH and BPCA-C6-P*p*OH can form H-bonds between the hydroxyl groups at the both ends of the dimers, thereby creating synclinic dimer tilting in the SmC, the highly ordered LC, and the crystalline phases. On the other hand, the free C═O stretching absorption in the carboxylic acids appears at 1737 cm^{-1} and the H-bonded C═O stretching absorption from the H-bonded cyclic dimers appears between 1683 and 1677 cm^{-1} as shown in Figure 6.[63−66] Except for BPCE-C6-P*m*OH,

(59) Takanishi, Y.; Takezoe, H.; Fukuda, A.; Komura, H.; Watanabe, J. *J. Mater. Chem.* **1992**, *2*, 71.
(60) Watanabe, J.; Komura, H.; Niiori, T. *Liq. Cryst.* **1993**, *13*, 455.
(61) Kishikawa, K.; Muramatsu, N.; Kohmoto, S.; Yamaguchi, K.; Yamamoto, M. *Chem. Mater.* **2003**, *15*, 3443.
(62) Huggins, K. E.; Son, S.; Stupp, S. I. *Macromolecules* **1997**, *30*, 5305.
(63) Stepanian, S. G.; Reva, I. D.; Radchenko, E. D.; Sheina, G. G. *Vib. Spectrosc.* **1996**, *11*, 123.
(64) Kutsumizu, S.; Kato, R.; Yamada, M.; Yano, S. *J. Phys. Chem. B* **1997**, *101*, 10666.
(65) Dong, J.; Ozaki, Y.; Nakashima, K. *Macromolecules* **1997**, *30*, 1111.
(66) Kutsumizu, S.; Yamada, M.; Yamaguchi, T.; Tanaka, K.; Akiyama, R. *J. Am. Chem. Soc.* **2003**, *125*, 2858.

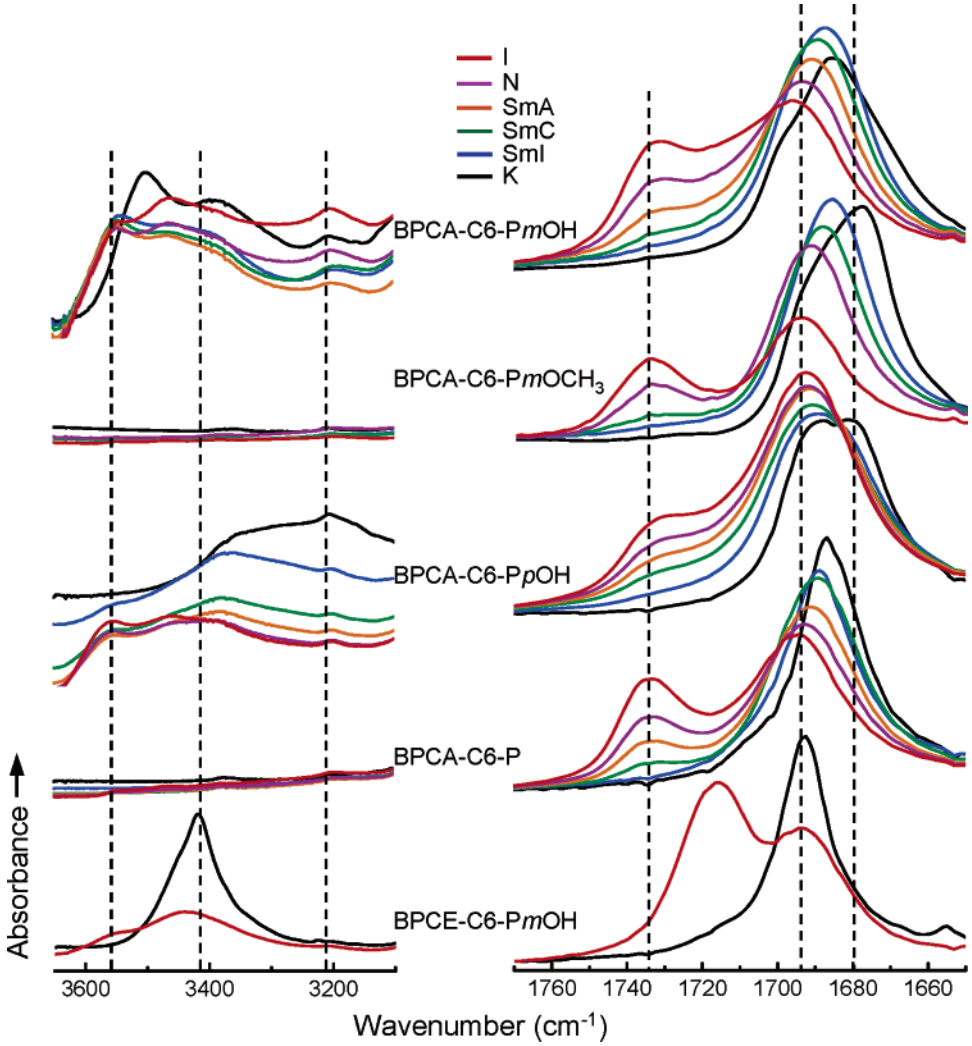

Figure 6. FT-IR spectra of achiral C6 biphenyl model compounds between 3650 and 3100 cm^{-1} and between 1770 and 1650 cm^{-1} at a cooling rate of 2.5 °C/min.

this series of compounds possess the head-to-head dimeric structure in these ordered LC and crystalline phases resulting from the intermolecular H-bonding between the carboxylic acids.

Chemical Origin of Helical Supramolecular Structures in the SmC Phases. This series of C6 model compounds, of which the carboxylic acid H-bonded dimers are the building blocks (expect for BPCE-C6-P*m*OH), forms the helical supramolecular structures as shown in Figure 7a−d under PLM, regardless of whether their dimers are synclinically or anticlinically tilted. Both right- and left-handed helical structures are observed in the same sample, when these compounds enter the SmC phase. Note that C6 biphenyl carboxylic acid compounds have neither the molecular chirality like the chiral molecules,[28−35] nor the significant bend like the banana-shaped molecules.[9−27] The angle between the long axis of the helical structure and twisted cylinder axis is not a constant for these compounds, indicating that the twisting power of these compounds is different. It is evident that the formation of dimers via the intermolecular H-bonding between carboxylic acids is the determining factor for the formation of the helical structure because BPCE-C6-P*m*OH does not exhibit a LC phase and no helical supramolecular structure forms. The existence of

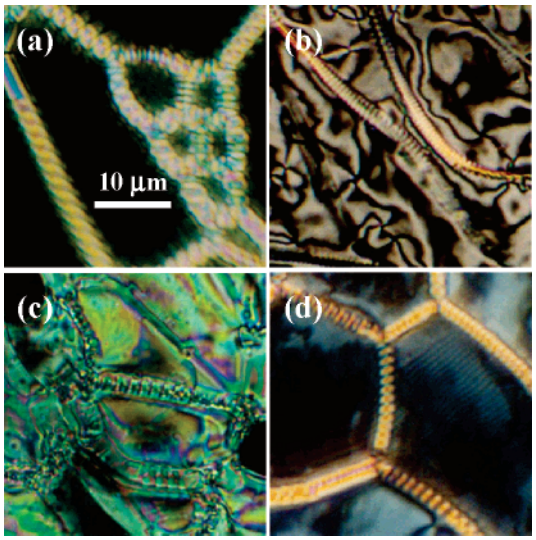

Figure 7. PLM helical supramolecular textures in the SmC phases of (a) BPCA-C6-P*m*OH, (b) BPCA-C6-P*p*OH, (c) BPCA-C6-P*m*OCH_3, and (d) BPCA-C6-P compounds.

the H-bonding between hydroxyl groups at the ends of dimers is critical to form the synclinic dimer tilting in the SmC_S phase, yet it is not a determining factor for the formation of the helical supramolecular structures, since both BPCA-C6-

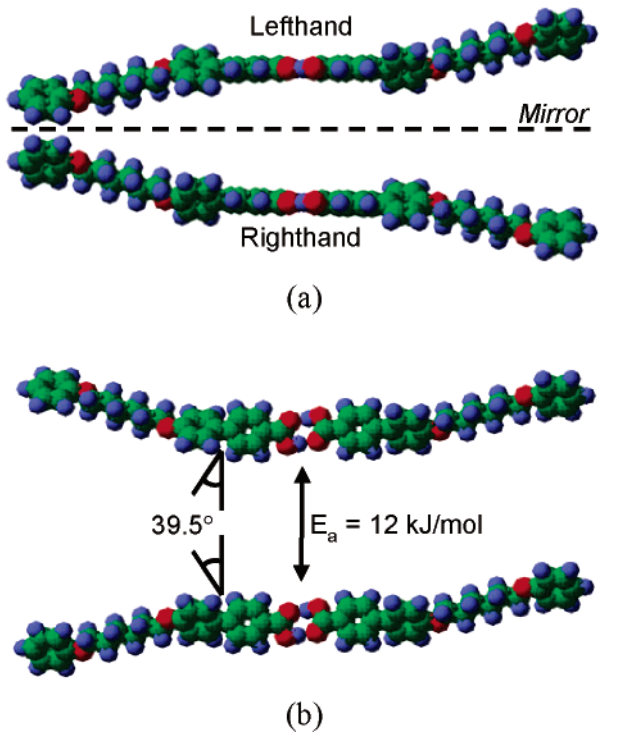

Figure 8. (a) Two enantiomeric minimal energy conformers of the head-to-head dimers of BPCA-C6-P in the isolated gas phase at 0 K using Cerius^2 4.6 and (b) the conformational changes with the calculated activation energy by rotating one of the planes at the end of the dimer with respect to the center plane of the dimer.

P*m*OCH$_3$ and BPCA-C6-P possess the anticlinic dimer tilting and form the helical structures. We know that without a phenyl group at each end of the dimers, the helical structure cannot be formed.[67] It is also known that in order to achieve a chiral property in racemic LC compounds, bulky terminal units (such as cyclohexane and cyclopentane) need to be introduced.[68,69] The chemical origin of the helical structure formation is thus due to the construction of the head-to-head dimers via the intermolecular H-bonding between carboxylic acid groups and the presence of phenyl groups at the ends of the dimers. The small "kinks" introduced by −OH or −OCH$_3$ groups at the meta-position of the phenyl groups are not critical, although it may affect the twisting power of the structures.

Computer simulation shows that the dimers possess a twist rather than a bent conformation, as illustrated in Figure 8a, which was carried out using Cerius^2 4.6 software. First, the global equilibrium conformation of BPCA-C6-P was determined at 0 K using the COMPASS force field as a representative example. The energy-minimized BPCA-C6-P was then used to construct the head-to-head dimer. The minimal energy conformation leads to the three rings at the center of the dimer being in the same plane. The alkoxyl chains are in the zigzag conformation, and they are in the same planes with the phenyl groups at each end of the dimer. These two planes at the both end sides of the dimer cross the center plane containing the three rings of the dimer at angles of ±39.5°. The activation energy to change from −39.5° to +39.5° is calculated to be ∼12 kJ/mol (Figure 8b). If the rotation of the three planes in this dimer is along the same direction, two enantiomeric conformers (axial chiral molecules) can be constructed as shown in Figure 8a. As long as these axial chiral conformers are thermodynamically stable at a certain temperature and pressure, we can consider them as an individual species, which can ultimately lead to the phase chirality (helical supramolecular structure).[6,31,32] The axial chiral conformers of the twisted head-to-head dimers with the end phenyl groups can be the chemical origin of the helical supramolecular structures in the SmC phases.

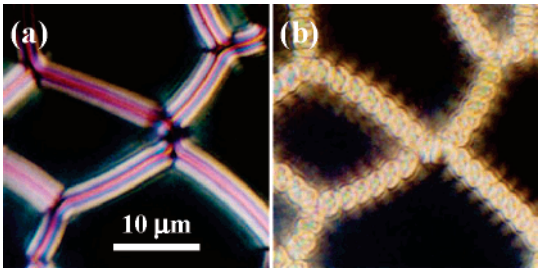

Figure 9. PLM textures in the (a) SmA and (b) SmC phases of BPCA-C6-P*m*OH at the cooling rate of 2.5 °C/min.

Physical Origin of Helical Supramolecular Structures in the SmC Phases. Figure 9a shows the cylinder network structure for the compound BPCA-C6-P*m*OH in the SmA phase. The helical supramolecular structure forms when the temperature enters the SmC phase as shown in Figure 9b. The 3D physical existence of the cylinder and helical structures was confirmed by the observations utilizing atomic force microscopy, scanning electron microscopy, and phase contrast optical microscopy in a previous report for BPCA-C8-P*m*OH.[1] The length of the cylinder between two junction points of the network structure in the SmA phase does not change when entering the SmC phase. The angle between the helical axis normal and the helical cylinder is 43 ± 5° for this compound. The helical formation along the long axis of the cylinder is either step-by-step or gradual.

The physical origin of this formation needs to be further investigated. The first task is to obtain reproducible 2D WAXD patterns of the helical structures. We found that the helical structure can be induced in the oriented thin film samples to form a mixture of helical and layer structures of BPCA-C6-P*m*OH. The result is shown in Figure 10a. The helical axis is aligned along the shear direction (*y*). A 2D WAXD pattern of this BPCA-C6-P*m*OH sample when the X-ray beam is aligned along the edge direction is shown in Figure 10b. In this pattern, in addition to the strong synclinic diffractions in the second and fourth quadrants which are attributed to the layered SmC_S phase structure, two relatively weak and diffused diffraction pairs close to the equator and the meridian (the circles in Figure 10b) can be observed with a weak ring pattern. All of these diffractions possess the identical 2θ value of 19.7°. An azimuthal scan of the 2D WAXD pattern in Figure 10b (between 2θ = 19.0° and 20.5°) is shown in Figure 10c. The two weak diffraction pairs are pointed out by the arrows in Figure 10c.

(67) Bahadur, B. *Liquid Crystals: Applications and Uses*; World Scientific: Singapore, 1990.
(68) Cowling, S. T.; Hall, A. W.; Goodby, J. W. *Chem. Commun.* **2005**, 1546.
(69) Cowling, S. T.; Hall, A. W.; Goodby, J. W. *Adv. Mater.* **2005**, *17*, 1077.

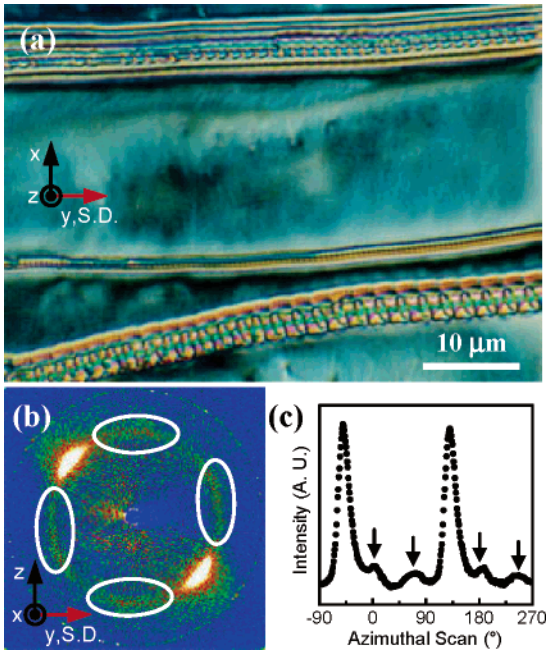

Figure 10. (a) PLM texture of the oriented BPCA-C6-P*m*OH sample of a mixed helical and layer structures and (b) its 2D WAXD pattern when the X-ray beam is along the edge direction; (c) an azimuthal scan of part b between $2\theta = 19°$ and 20.5°.

To understand the origin of these two weak diffraction pairs, the crystallographic analysis of the molecular orientation in the helical supramolecular structure of the SmC phase is utilized. The schematic molecular orientations in the layered SmC phase and in the helical structure are illustrated in Figure 11, parts a and c, respectively. In Figure 11c, cross-sectional schemes of molecular arrangements inside the helical structure are illustrated, and they are slices from the cut along the helical axis at the front, the center, and the back. The predicted 2D WAXD patterns are shown in Figure 11b for the layer structure, which agrees with the experimental observations in the 2D WAXD pattern, as shown in Figure 3b. The front and the back slices of the helical structures can generate two diffused diffractions close to the equator and the meridian, but the slice at the center only exhibits a diffused ring pattern, as shown in Figure 11d. On the basis of this mixed model of the layer and helical structures, the predicted 2D WAXD pattern is shown in Figure 11e, which is qualitatively identical with that of the experimental result shown in Figure 10b.

The morphological change from the cylinder in the SmA to the helix in the SmC is speculated to involve a physical mechanism based on the dimer tilting as shown in Figure 12a−c, assuming that the long axis of the dimers in the cylinder is oriented parallel to the cylinder surface normal in the SmA phase, which is often observed in Myelin textures (Figure 12a).[6,32] They tilt toward the long axis of the cylinder when entering the SmC phase with a dimer tilting angle, θ. The cylinders then elongate with the assumptions of volume invariance (assuming that the density change between the SmA and SmC phases are small) and no mass transfer between cylinders and their surroundings (Figure 12b). The dimer tilting leads to a reduction in the cylinder diameter (d). Since the cylinder length (L) in the SmA phase is fixed between two neighboring junction points in the network as

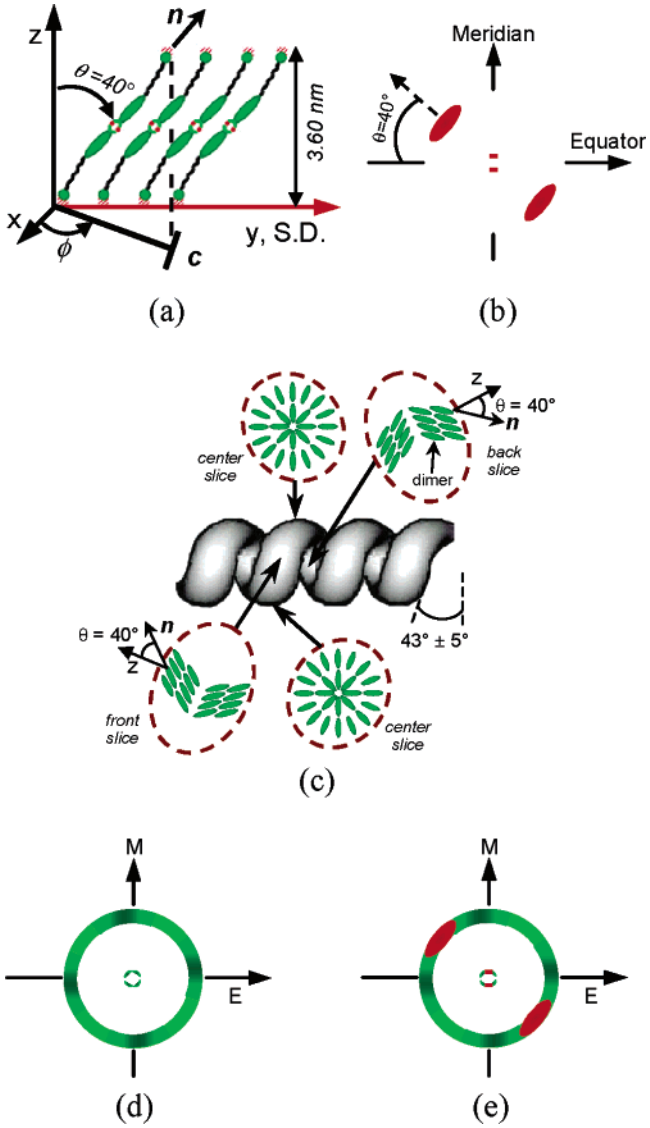

Figure 11. (a) Schematic illustration of the molecular orientation in the SmC layers and (b) its predicted 2D WAXD pattern; (c) schematic illustration of the molecular orientation in the helix and (d) its predicted 2D WAXD pattern; (e) the predicted 2D WAXD pattern for the mixture of the layer and helical structures. In part a, ***n*** is the molecular director with an average tilt angle (θ) from the layer normal (z), ***c*** is the unit vector giving the projection of ***n*** on the layer plane ($x-y$ plane), and ϕ is the azimuthal twist angle.

shown in Figure 9, parts a and b, the elongation of the cylinders generates a mechanical compression to force the cylinder twisting and leads to the formation of the helical structure. Figures 12c is the schematic illustration for the twisted helical supramolecular structure.

A quantitative analysis of this physical explanation for the helical structure formation can be conducted by comparing the proposed physical model and experimental observations. Similar to the case of helical structures in chiral molecules,[31−35,70] the helical structure in this system is constructed by nonparallel packing of the dimeric axial conformers with their neighbors in the SmC phase. Since the average dimer axis is tilted relative to the layer normal with a tilting angle of $\theta = 40°$ (Figure 3b) for BPCA-C6-

(70) Lotz, B.; Vassal, A. G.; Brack, A.; Magoshi, J. *J. Mol. Biol.* **1982**, *156*, 345.

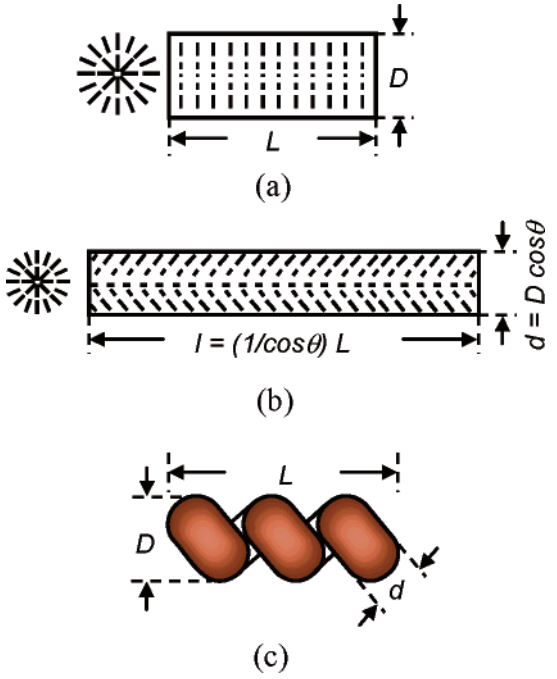

Figure 12. Schematic illustration of the molecular arrangement in (a) the SmA cylinder and in (b) the elongated cylinder of the SmC phase and of (c) the single helix.

P*m*OH, the favored twist ($\Delta\phi$ = a local average scalar azimuthal twist angle) from one to its neighbor can lead the helical structure. On the basis of the morphological helical geometry dimensions (Figure 9b) and the average lateral distance of neighboring dimers within the layer as measured by the WAXD experiments (0.451 nm, see Figure 3b), one can calculate the twisting angle ($\Delta\phi$) of neighboring dimers in the helical structure for this compound. The morphological average pitch length of the helical structure is 4.2 μm, and its average length of the cylinder which constructs the helix is 6.2 μm. Here, the length of cylinder in one pitch length of helix can be also calculated based on the molecular aspect as described in the physical origin of helical structure formation (Figure 12b): $l = L/\cos\theta = 4.2\ \mu\text{m}/\cos(40°) = 5.5\ \mu\text{m}$. The difference between the calculated (5.5 μm) and experimental (6.2 μm) data can come from the simple assumptions of constant density and no mass transfer between cylinders and their surroundings for this model. To fill the length of helical cylinder in the morphological pitch length of the helix, about 14 000 dimers are needed. Since the dimers are symmetric, dimers are going to rotate 180° continuously in the morphological pitch length of the helical supramolecular structures. Therefore, the local twisting angle ($\Delta\phi$) from neighbor to neighbor within the layer is about 0.013°. This local twisting angle which was calculated based on the WAXD and morphological observations in PLM is on the same order as that of other chiral systems.[33−35,70]

Conclusion

To understand the formation mechanism of helical supramolecular structures in the SmC_S phase of achiral BPCA-C*n*-P*m*OH ($n = 6-10$), a series of newly designed achiral C6 biphenyl carboxylic acid compounds has been synthesized. The phase behaviors and structures of this series of compounds were characterized using the combined techniques of DSC, PLM, WAXD, and SAED. The H-bond formation between carboxylic acids as well as between hydroxyl groups was also studied using FT-IR. With the exception of BPCE-C6-P*m*OH, the achiral C6 biphenyl carboxylic acid compounds form helical structures during the transition from the SmA to the SmC phases. The self-assembled twisted dimers with the phenyl end groups are essential to form the stable helical supramolecular structure. The existence of the −OH groups at the meta- or para-position of the phenyl groups determines the synclinic or anticlinic packing of the dimers, while they are not critical to the formation of the helical supramolecular structures. Even in BPCA-C6-P*m*OCH_3 and BPCA-C6-P which cannot form H-bonds between the neighboring layers, the helical structure can still be formed. Computer simulation indicates that the dimers possess a twist rather than a bent conformation with a ~12 kJ/mol activation energy. This twist does not exist in the BPCE-C6-P*m*OH compound which cannot form the dimers. Since in the case of the dimers without the phenyl groups at the ends no helical structure can be formed, we can conclude that the chemical origin of the formation of these helical structures is due to the axial chiral conformers of individual head-to-head dimers with phenyl groups at the both ends. The physical origin is that the LC cylinders in the SmA phase are under the mechanical compression caused by dimer tilting toward the long axis of the LC cylinders in the networks when entering the SmC phases.

Acknowledgment. This work was supported by NSF DMR-0516602. We also acknowledge Perkin-Elmer Co. for their support in providing a Diamond DSC instrument for our laboratory.

Supporting Information Available: The crystal and highly ordered LC structure determinations for the series of achiral C6 biphenyl carboxylic acid compounds (PDF). This material is available free of charge via the Internet at http://pubs.acs.org.

CM0518832